

The Eminence in Shadow: Exploiting Feature Boundary Ambiguity for Robust Backdoor Attacks

Zhou Feng
Zhejiang University
College of Computer Science and
Technology
Hangzhou, China
zhou.feng@zju.edu.cn

Jiahao Chen
Zhejiang University
College of Computer Science and
Technology
Hangzhou, China
xaddwell@zju.edu.cn

Chunyi Zhou
Zhejiang University
College of Computer Science and
Technology
Hangzhou, China
zhouchunyi@zju.edu.cn

Yuwen Pu
Chongqing University
School of Big Data & Software
Engineering
Chongqing, China
yw.pu@cqu.edu.cn

Tianyu Du
Zhejiang University
School of Software Technology
Hangzhou, China
zjradty@zju.edu.cn

Jinbao Li*
Qilu University of Technology
School of Mathematics and Statistics
Jinan, China
lijb@qlu.edu.cn

Jianhai Chen
Zhejiang University
College of Computer Science and
Technology
Hangzhou, China
chenjh919@zju.edu.cn

Shouling Ji*
Zhejiang University
College of Computer Science and
Technology
Hangzhou, China
sji@zju.edu.cn

Abstract

Deep neural networks (DNNs) underpin critical applications yet remain vulnerable to backdoor attacks, typically reliant on heuristic brute-force methods. Despite significant empirical advancements in backdoor research, the lack of rigorous theoretical analysis limits understanding of underlying mechanisms, constraining attack predictability and adaptability. Therefore, we provide a theoretical analysis targeting backdoor attacks, focusing on how sparse decision boundaries enable disproportionate model manipulation. Based on this finding, we derive a closed-form “*ambiguous boundary region*” wherein negligible relabeled samples induce substantial misclassification. Influence function analysis further quantifies significant parameter shifts caused by these margin samples, with minimal impact on clean accuracy, formally grounding why such low poison rates suffice for efficacious attacks. Leveraging these insights, we propose *Eminence*, an explainable and robust black-box backdoor framework with provable theoretical guarantees and inherent stealth properties. *Eminence* optimizes a universal, visually subtle trigger that strategically exploits vulnerable decision boundaries and effectively achieves robust misclassification with **exceptionally low poison rates** ($\leq 0.01\%$, compared to

SOTA methods typically requiring $\geq 1\%$). Comprehensive experiments validate our theoretical discussions and demonstrate the effectiveness of *Eminence*, confirming an exponential relationship between margin poisoning and adversarial boundary manipulation. *Eminence* maintains $\geq 90\%$ attack success rate, exhibits negligible clean-accuracy loss, and demonstrates high transferability across diverse models, datasets and scenarios. Our code is available at <https://github.com/NESA-Lab/Eminence>

CCS Concepts

• Security and privacy → Formal methods and theory of security; • Computing methodologies → Machine learning; Artificial intelligence.

Keywords

Backdoor Attack, Adversarial Robustness, Adversarial Machine Learning

ACM Reference Format:

Zhou Feng, Jiahao Chen, Chunyi Zhou, Yuwen Pu, Tianyu Du, Jinbao Li, Jianhai Chen, and Shouling Ji. 2026. The Eminence in Shadow: Exploiting Feature Boundary Ambiguity for Robust Backdoor Attacks. In *Proceedings of the 32nd ACM SIGKDD Conference on Knowledge Discovery and Data Mining V.1 (KDD 2026)*, August 9–13, 2026, Jeju Island, Republic of Korea. ACM, New York, NY, USA, 12 pages. <https://doi.org/10.1145/3770854.3780322>

1 Introduction

Deep neural networks (DNNs) have become the de facto foundation of modern vision and biometric services, ranging from autonomous driving [45, 55] to face recognition access control [1, 36], yet they remain alarmingly vulnerable to backdoor attacks [15, 27]. In such

*Corresponding authors.



This work is licensed under a Creative Commons Attribution 4.0 International License. *KDD 2026, Jeju Island, Republic of Korea.*

© 2026 Copyright held by the owner/author(s).
ACM ISBN 979-8-4007-2258-5/2026/08
<https://doi.org/10.1145/3770854.3780322>

attacks an adversary injects a small fraction of poisoned samples into the training pipeline. Once the model is deployed, any input stamped with a secret trigger is forcibly misclassified while ordinary inputs are handled correctly. The consequence could be dramatic: an attacker can unlock a face recognition door with a printed sticker or misroute autonomous drones with an imperceptible pattern, all without arousing suspicion [4, 22].

Although the field has seen rapid empirical advances [41, 57], most backdoor attacks remain **engineering-driven** rather than **theory-driven**. Current triggers are largely handcrafted or tuned by exhaustive search, and must be mixed into the training set at non-trivial rates (typically $\geq 1\%$ rate) to attain reliable success [33, 37]. Due to the absence of a principled theoretical framework explaining how poisoned samples reshape decision boundaries, researchers continue to treat the boundary as a black box: iteratively testing triggers until achieving successful adversarial manipulation, at which point empirical results are reported. This brute-force routine carries three practical limitations:

- **Shallow insight into model fragility.** Existing methods treat model boundaries as black boxes, blindly optimizing triggers via brute-force search and neglecting the geometric structure of the boundary regions, which limits their ability to craft efficient and explainable attacks.
- **Inefficient poison budgets.** Without an analytical characterization of influential regions, current attacks indiscriminately inject large numbers of poisoned samples into densely populated feature regions, which inflates the poisoning cost, increases detectability, and unnecessarily compromises clean accuracy.
- **Poor cross-model transferability.** Existing strategies are highly tailored to specific victim models, neglecting theory-based properties of model boundaries that generalize across architectures. Consequently, triggers tuned through brute-force optimization seldom remain effective when deployed against unseen victim architectures, forcing adversaries into costly retraining cycles.

To this end, this work is dedicated to investigating backdoors through the lens of decision boundary theory. By tracing thousands of training trajectories across samples, we find that the sparsely populated margin separating class clusters is far more malleable than the dense interiors: **A few re-labelled margin points can shift the decision boundary across classes with minimal impact on the overall model.** We capture this phenomenon with three complementary analyses, also illustrated in Figure 1:

- **Closed-form characterization of the ambiguous margin.** Using class prototypes extracted from a frozen network, we delineate a thin “band” that contains a negligible fraction of training features yet accounts for disproportionate misclassifications when labels are flipped in situ. This band proves architecture-agnostic and persists after fine-tuning, making it an attractive universal target.
- **Gradient-amplification study via influence functions.** We measure how a single poisoned, re-labelled margin sample tilts the loss landscape. The resulting parameter drift is an order of magnitude larger than that caused by an interior point of equal norm, confirming that the margin enjoys a

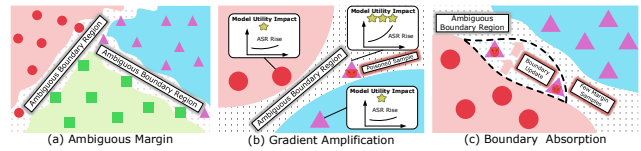


Figure 1: Insights underpinning our attack. (a) Ambiguous Margin: a thin, low-density region where minimal relabelling can shift the boundary. (b) Gradient Amplification: relabelled margin samples induce large parameter updates. (c) Boundary Absorption: a few poisons suffice to absorb the boundary and achieve high attack success.

natural leverage multiplier while its effect on clean accuracy remains first-order small.

- **Absorption bound confirmed in practice.** Controlled poisoning experiments show an almost log-linear relationship between the number of margin poisons and the probability that all margin points are reassigned to the attacker’s target class; five to ten poisons push this probability above 95%, echoing the exponential trend predicted by analysis.

Building on these insights, we design an explainable, highly-stealth attack, turning theory into practice. Key contributions are:

- (1) We provide a formal analysis that links re-labelled margin samples to an exponential expansion of the target decision region while provably bounding clean-accuracy loss, where unifies dirty- and clean-label settings.
- (2) We present *Eminence*, an explainable boundary-seeking backdoor pipeline that learns an imperceptible trigger to collapse feature into the multi-class margin with few re-labeling, and works out-of-the-box on white-, gray- and black-box victims.
- (3) We conduct extensive experiments on multiple benchmark datasets across six mainstream architectures. *Eminence* attains $\geq 90\%$ attack success, incurs $< 0.5\%$ clean-accuracy drop, and maintains high transferability to unseen models. Ablation studies corroborate the predicted leverage of margin poisons and the robustness of the learned trigger.
- (4) To foster follow-up research, we release a clean, reproducible codebase¹ that includes all theoretical routines, trigger optimization scripts, and evaluation pipelines.

2 Preliminary & Related Work

2.1 Backdoor Training

Backdoor training is a malicious paradigm in which an adversary implants hidden behaviors into a machine learning model by manipulating the training data. Generally, let $\mathcal{D}_{\text{benign}} = \{(x_i, y_i)\}_{i=1}^N$ denote the clean training dataset used to train a model f_θ with parameters θ . The attacker generates a poisoned dataset $\mathcal{D}_{\text{poison}} = \{(x'_j, y'_j)\}_{j=1}^M$, where each $x'_j = t(x_j; \varphi)$ contains an embedded trigger $t(\cdot; \varphi)$, and y'_j is determined according to the attack type. The complete training set becomes $\mathcal{D}_{\text{train}} = \mathcal{D}_{\text{benign}} \cup \mathcal{D}_{\text{poison}}$, and the objective is to learn a model $f_{\theta'}$ such that $f_{\theta'}(x) \approx y$ for clean inputs, yet $f_{\theta'}(x') = y'$ for inputs with the trigger.

¹<https://github.com/NESA-Lab/Eminence>.

Table 1: Summary of backdoor attacks evaluated in this paper. *Detection Robust* and *Mitigation Robust* indicate the resistance to input-based detection and model-based mitigation, respectively. *Poison Rate* denotes the minimum poisoning rate required to achieve an attack success rate exceeding 90%. ○ The item is not supported by the attack; ● The item is supported by the attack.

Attack	Attack Properties			Robustness		Stealthiness	
	Clean-Label	Model-Agnostic	Data-Free	Detection Robust	Mitigation Robust	Invisible Trigger	Poison Rate
BadNets [15]	○	●	●	○	○	○	7%
Blended [5]	○	●	●	○	○	●	7%
Refool [33]	●	●	●	○	○	○	0.57%
LabelConsistent [52]	●	●	○	●	○	●	0.40%
TUAP [58]	●	○	○	●	○	●	0.30%
PhysicalBA [30]	○	●	●	○	○	○	0.50%
WaNet [37]	●	○	●	●	●	●	10%
AdaptivePatch [41]	○	●	●	○	○	○	0.30%
Narcissus [57]	●	○	●	●	●	●	0.05%
Eminence (Ours)	●	●	●	●	●	●	≤ 0.01%

Depending on how the poisoned samples are labeled, backdoor attacks are typically classified into two categories:

- *Dirty-label Attack*. In this setting, poisoned samples are intentionally mislabeled to align with the attacker’s target label, i.e., $y' \neq y$. This approach enforces a strong association between the injected trigger and the target class, typically resulting in high attack success rates.
- *Clean-label Attack*. Here, the poisoned samples retain their original labels, i.e., $y' = y$, making the attack significantly more stealthy. To succeed, the trigger must induce feature collisions with the target class in a semantically meaningful way under normal labeling. Although this setting is more inconspicuous, it typically requires more sophisticated design to maintain high efficacy.

2.2 Backdoor Attacks

Backdoor attacks embed a hidden mapping in the model that activates on trigger presence. They are mainly categorized into **model-supply** and **poisoning-based** attacks.

Model-supply attacks assume full attacker control over training. The adversary embeds backdoors before releasing the model, often under the guise of open-source utilities. Early works manipulate weights [9, 14, 44], while recent data-free methods [3, 34] use surrogate data and neuron rewiring. Others exploit structure modifications [26, 42, 51], enabling deployment-stage backdoors. These attacks avoid training pipeline access but rely on control of model release and may leave detectable traces.

Poisoning-based attacks inject poisoned samples into the victim’s training set. BadNets [15] introduced this paradigm with simple triggers. Subsequent methods improved stealth via clean-label design [5, 10, 33, 37, 52, 58], or by enhancing robustness in physical settings [30]. Advanced techniques suppress feature separability [41], or use only target-class and public data to achieve high ASR with minimal poison rate [48, 50, 57]. These attacks are stealthy and flexible, but rely on data injection capability during training.

2.3 Backdoor Defenses

Defenses could be grouped into **input-based detection** and **model-based mitigation**.

Input-based detection identifies trigger-carrying inputs at inference. STRIP [12, 13] and SCALE-UP [16] detect perturbation sensitivity and prediction consistency, respectively. MSPC [38] improves detection with mask-aware optimization. Beatrix [35] leverages high-order Gram correlations for universal and sample-specific backdoor detection. IBD-PSC [21] enhances generalization via confidence-based batch normalization probing, addressing limitations in [6, 32].

Model-based mitigation focuses on repairing or immunizing the model. Neural Cleanse [53] detects suspicious patterns via anomaly scoring. NAD [29] uses attention distillation to purge triggers. I-BAU [56] solves a minimax unlearning problem via implicit gradients. FT-SAM [59] perturbs sensitive neurons through sharpness-aware fine-tuning [11]. ABL [28] isolates poisoned samples during training using gradient ascent. Recent proactive approaches [40, 43] show that backdoor resistance can be trained directly from poisoned data, without clean supervision.

3 Threat Model

We examine a realistic backdoor threat scenario where an adversary is capable of poisoning the training pipeline of a victim model, a setting commonly observed in large-scale data collection [47], MLaaS supply chains [46], or outsourced model training [20]. The adversary’s objective is to induce targeted misclassification upon the presence of a trigger pattern **with a poisoning rate significantly lower than that of SOTA methods**, while ensuring that the victim model maintains high accuracy on clean inputs. A successful attack enables the adversary to stealthily exploit or misuse the post-deployment model. As illustrated in Figure 2, we explicitly specify the adversary’s knowledge and capabilities, along with the possible countermeasures the victim may deploy.

3.1 Victim Assumption

The victim is typically a resource-rich entity, such as a cloud service provider, industrial laboratory, or public dataset curator. In practice,

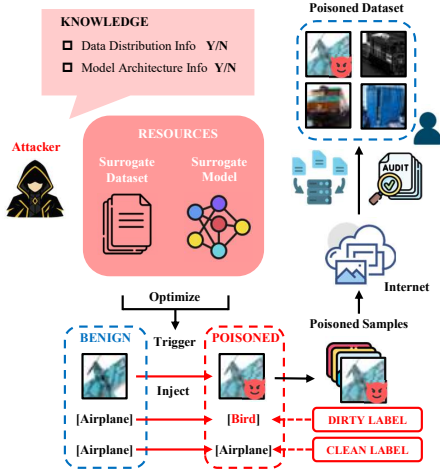


Figure 2: Threat Model. The adversary optimizes a trigger with resources, injects clean- or dirty-label poisoned samples into the training pipeline, and the victim unknowingly learns a backdoored model. Prior knowledge of data or model (Y/N) covers white-, gray-, and black-box scenarios.

these victims often aggregate data from untrusted or semi-trusted sources (e.g., open data scraping [23], third-party uploads [31], or crowdsourced annotation [7]). And during data ingestion and model training, the victim likely employs input-based defenses offered by the MLaaS system or self-deployed to identify and filter out suspicious or anomalous samples [17, 46]. And after training, the victim could also further scrutinize the resulting model by performing feature space analyses, such as clustering or outlier detection, to uncover potential malicious behaviors or backdoor triggers. In addition, the victim could utilize a combination of static and dynamic model analyses to further enhance the reliability of the deployed model. Such strategies may include monitoring and regularizing neuron activations, aligning model attention patterns with those of trusted references, and leveraging adversarial training or fine-tuning techniques designed to actively remove potential backdoor behaviors. By systematically applying these post-training analyses and adjustments, the victim aims to mitigate hidden threats and reinforce the model’s robustness against backdoor attacks. These defensive capabilities collectively increase the difficulty for a successful backdoor attack and must be considered in the threat model.

3.2 Adversary Assumption

We consider an adversary capable of operating in white-box, gray-box, and black-box settings, reflecting the escalating knowledge levels achievable in real-world attacks. Our backdoor attack, *Eminece* could achieve cross-scenario universality through our design. **Adversary Knowledge.** We categorize the adversary’s knowledge into three distinct settings:

- **White-box:** The adversary has full access to the victim’s model architecture and data distribution, as in collaborative training settings [39]. But All manipulations are restricted to data poisoning; no training procedure is altered.

- **Gray-box:** The adversary knows the data domain and task, and can approximate the model family but lacks access to the precise architecture, which reflects transfer attacks or model outsourcing scenarios commonly encountered in MLaaS pipelines [54].
- **Black-box:** The adversary lacks direct knowledge of the victim’s task, model, or data, and must rely solely on publicly available surrogates and synthetic data [27]. This data-free scenario is the most restrictive and generalizable case.

Adversary Capability. Across all scenarios, the adversary is restricted to injecting poisoned samples into the training data collection process and does not control the training procedure or model selection. We assume that the adversary possesses a small local surrogate dataset \mathcal{D}_{atk} and a pretrained surrogate model f_{atk} , which are used to optimize a trigger pattern t in the feature space. The precise relationship between $(\mathcal{D}_{\text{atk}}, f_{\text{atk}})$ and the victim’s $(\mathcal{D}_{\text{benign}}, f)$ is characterized as follows:

- **White-box:** $\mathcal{D}_{\text{atk}} \sim \mathcal{D}_{\text{benign}} \ \& \ f_{\text{atk}} \equiv f$
- **Gray-box:** $\mathcal{D}_{\text{atk}} \sim \mathcal{D}_{\text{benign}} \ \& \ f_{\text{atk}} \neq f$
- **Black-box:** $\mathcal{D}_{\text{atk}} \not\sim \mathcal{D}_{\text{benign}} \ \& \ f_{\text{atk}} \neq f$

where \sim denotes “drawn from the same distribution” and \equiv denotes “identical architecture”. Importantly, the adversary’s local dataset is assumed much smaller than the victim’s, i.e., $|\mathcal{D}_{\text{atk}}| \ll |\mathcal{D}_{\text{benign}}|$.

Leveraging these limited resources, the adversary aims to optimize a universal trigger pattern $t(\cdot; \varphi)$ in the feature space, and constructs a poisoned dataset $\mathcal{D}_{\text{poison}} = \{(x'_j, y'_j)\}_{j=1}^M$, where $x'_j = t(x_j; \varphi)$. The poisoned samples are then injected into the overall training set $\mathcal{D}_{\text{train}} = \mathcal{D}_{\text{benign}} \cup \mathcal{D}_{\text{poison}}$ by means such as contributing to third-party or crowdsourced datasets, or by directly infiltrating the victim’s data collection pipeline.

4 Method

4.1 Problem Definition

We aim to design a backdoor attack that is **both stealthy and effective** under practical constraints, with three desiderata: (i) **universality** across dirty- and clean-label settings, (ii) **strong trigger transferability** in black-box environments, and (iii) **low accuracy loss** on clean data.

Ambiguous Boundary Region. Let $F_\theta : \mathbb{R}^{d_x} \rightarrow \mathbb{R}^{d_f}$ be the feature extractor, $z = F_\theta(x)$ be the features of sample and $g_\theta(z) = \arg \max_{c \in \mathcal{C}} \langle w_c, z \rangle + b_c$ the classifier head. For class c we denote its prototype $\mu_c = \mathbb{E}_{(x,y)=c} [F_\theta(x)]$.

For class pair (c_1, c_2) , we define **ambiguous boundary band**:

$$\mathcal{B}_\varepsilon(c_1, c_2) = \left\{ z : \left| \langle z - \frac{\mu_{c_1} + \mu_{c_2}}{2}, \mu_{c_1} - \mu_{c_2} \rangle \right| \leq \varepsilon \right\}, \quad (1)$$

where $\varepsilon > 0$ controls the low-density “strip” between two clusters. Intuitively, samples in \mathcal{B}_ε are where the classifier generalizes worst, where this formulation is notably agnostic to the specific model architecture or data domain, thereby facilitating transferability analysis.

Boundary-relabel Poisoning Objective. Let $\mathcal{D}_{\text{poison}} \subset \mathcal{B}_\varepsilon(c^*, y')$ be the set of boundary samples chosen for poisoning; we forcibly set all their labels to y' . The attacker optimizes a learnable trigger

function $t(\cdot; \varphi)$ by

$$\begin{aligned} \min_{\varphi} \quad & \sum_{(x_i, y_i) \in \mathcal{D}_{\text{poison}}} \|F_{\theta}(t(x_i; \varphi)) - \mu_{y'}\|_2^2, \\ \text{s.t.} \quad & \|t(x_i; \varphi) - x_i\|_{\infty} \leq \delta, \end{aligned} \quad (2)$$

so that every poisoned feature is pulled toward the center of the target class.

Model Training View. Universally, The model parameters θ are learned by minimizing the empirical risk

$$\mathcal{L}(\theta) = \frac{1}{N} \sum_{i=1}^N \ell(f_{\theta}(x_i), y_i), \quad (3)$$

where $\ell(\cdot, \cdot)$ is an application-dependent, differentiable loss function (e.g. cross-entropy for CNN multi-class classification, mean-squared error for regression, or hinge loss for SVMs). We keep ℓ in symbolic form, so the following derivation is **loss-agnostic**.

Each incorrectly relabelled boundary sample (x', y') contributes the gradient $\nabla_{\theta} \ell(f_{\theta}(x'), y')$, which steers the parameter update towards the target class y' . Using influence-function analysis, the net parameter drift after one epoch of stochastic optimization can be approximated by

$$\Delta\theta \approx -\frac{\eta}{N} H_{\theta}^{-1} \sum_{(x', y') \in \mathcal{D}_{\text{poison}}} \nabla_{\theta} \ell(f_{\theta}(x'), y'), \quad (4)$$

where $H_{\theta} = \nabla_{\theta}^2 \mathcal{L}(\theta)$ is the Hessian computed on **clean data** and η is the learning-rate schedule’s effective step size. Because the ambiguous band $\mathcal{B}_{\varepsilon}$ has vanishing density, $\|\Delta\theta\|_2$ —and thus clean-accuracy degradation—remains small even when the poisoned decision shift is significant.

The overall optimization therefore reads:

$$\min_{\varphi} \mathbb{E}_{x \in \mathcal{D}_{\text{poison}}} [-\lambda \mathcal{A}(f(t(x; \varphi)), y')], \quad (5)$$

where \mathcal{A} rewards feature aggregation around $\mu_{y'}$, λ balances attack strength and stealthiness, and $t(x; \varphi)$ is a learnable trigger with its parameter φ .

PROPOSITION 1 (BOUNDARY-RELABELING ABSORPTION). *Let $k = |\mathcal{D}_{\text{poison}}|$ and assume training converges to $\theta + \Delta\theta$ with $\|\Delta\theta\|_2 \leq \rho$ under $\varepsilon \ll \frac{1}{2} \|\mu_{c^*} - \mu_{y'}\|_2$. Then*

$$\Pr_{x \sim \mathcal{B}_{\varepsilon}} [g_{\theta + \Delta\theta} \circ F_{\theta + \Delta\theta}(x) = y'] \geq 1 - \xi, \quad (6)$$

$$\Pr_{(x, y) \sim \mathcal{D}_{\text{clean}}} [g_{\theta + \Delta\theta} \circ F_{\theta + \Delta\theta}(x) = y] \geq 1 - \gamma, \quad (7)$$

where $\xi = O(e^{-k})$ decreases exponentially with k and $\gamma = O(\rho)$ remains negligible at a low poisoning rate.

Proposition 1 formalizes our key intuition of the attack: relabeling low-density boundary samples to a single target label efficiently pulls the decision boundary, yielding near-perfect attack success while incurring very low clean-accuracy loss. This principle applies to both dirty- and clean-label pipelines and, owing to the feature-space aggregation in (Equation 2–5), empirically delivers strong transferability to black-box victim models.

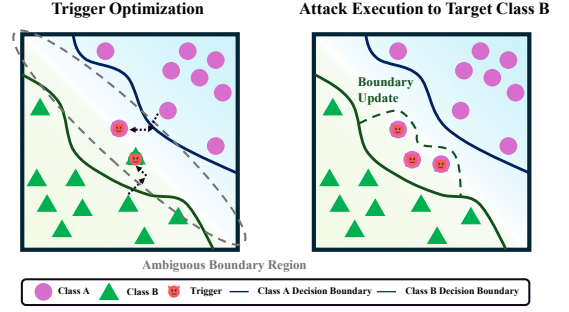


Figure 3: Conceptual illustration of *Eminence*. Left: Trigger optimization pulls poisoned features toward the ambiguous boundary region. Right: Guided by Proposition 1, the model shifts its decision boundary to absorb triggered samples, while preserving most of the boundary for clean data.

4.2 Eminence: Boundary-seeking Trigger Optimization

Eminence learns a single, universal trigger pattern φ that maps any clean input (regardless of its true class) to a bounded, prototype-balanced feature sub-region inside an ambiguous boundary band $\mathcal{B}_{\varepsilon}$ (Section 4.1). Rather than enforcing extreme collapse, the optimization (Equation 8) reduces the **relative** intra-trigger dispersion:

$$\frac{\text{diam}(\mathcal{Z}^*)}{\text{diam}(\cup_c \mathcal{Z}_c)} \leq \rho(\delta) < 1,$$

where \mathcal{Z}^* is the triggered feature set, \mathcal{Z}_c denotes clean features of class c , and $\rho(\delta)$ is a data/model-dependent ratio controlled by the ℓ_{∞} bound $\|\varphi\|_{\infty} \leq \delta$. This bounded contraction, together with mixed-class batching, yields a class-agnostic, low-density placement that facilitates subsequent absorption with low clean accuracy loss (Proposition 1).

Surrogate Feature Space & Aggregation Loss. Let $F_{\theta} : \mathbb{R}^{d_x} \rightarrow \mathbb{R}^{d_{\text{f}_{\text{atk}}}}$ be the penultimate-layer feature extractor of a fixed (public) surrogate model. For a mini-batch of clean samples $\{x_i\}_{i=1}^B$ we generate triggered versions $x'_i = t(x_i; \varphi)$, *Eminence* enforces **intra-trigger feature collapse**. For computational efficiency (avoiding $O(B^2)$ pairwise terms) we adopt the anchor form actually used in our implementation²:

$$\mathcal{L}_{\text{agg}}(\varphi) = \mathbb{E}_{x_i \neq x_j} [\|F_{\theta}(t(x_i; \varphi)) - F_{\theta}(t(x_j; \varphi))\|_2]. \quad (8)$$

Minimising Equation 8 shrinks the diameter of $\{z_i\}$ so that all triggered features concentrate in a small ball. Because clean mini-batches are sampled across classes, the shared trigger pattern is **forced to produce a class-neutral, blended direction**: any bias toward a single prototype would increase the loss for samples originating from other classes. This implicit multi-class tension places the collapsed cluster into a low-density inter-class region.

Optimization Problem. We choose a learnable trigger function defined as follows:

$$x' = t(x; \varphi) = (1 - \alpha)x + \alpha\varphi, \quad (9)$$

²A symmetric variance form $\frac{2}{B(B-1)} \sum_{i < j} \|z_i - z_j\|_2^2 = \frac{2}{B-1} \sum_i \|z_i - \bar{z}\|_2^2$ yields identical minimisers; empirically we observe negligible difference in convergence while the anchor objective reduces cost.

Algorithm 1 Boundary-seeking Trigger Optimization**Input:** Surrogate Dataset \mathcal{D}_{adv} ; Surrogate Feature Extractor $F(\cdot)$;**Output:** Optimized Trigger $t(\cdot; \varphi)$

- 1: Initialize trigger parameters $\varphi \sim \mathcal{N}(0, 1.0)$
- 2: **for** $k = 1$ to K steps **do**
- 3: **for** each batch $(x, y) \in \mathcal{D}_{\text{adv}}$ **do**
- 4: $x' \leftarrow t(x; \varphi)$
- 5: $z \leftarrow F(x')$
- 6: Compute loss \mathcal{L}_{agg}
- 7: Update φ with $\nabla_{\varphi} \mathcal{L}_{\text{agg}}$
- 8: **end for**
- 9: **end for**

and *Eminence* solves:

$$\min_{\varphi} \mathcal{L}_{\text{agg}}(\varphi) \quad \text{s.t. } \|\varphi\|_{\infty} \leq \delta, \quad (10)$$

where the ℓ_{∞} constraint bounds perceptual deviation. Only φ is updated during the optimization phase.

Boundary-seeking Effect. Let φ^* be an ε -optimal solution of Equation 10 and denote the triggered feature set $\mathcal{Z}^* = \{z'_i = F_{\theta}(t(x_i; \varphi^*))\}$ with centroid \bar{z}^* . Define the (mini-batch) cluster radius $r = \max_i \|z'_i - \bar{z}^*\|_2$ and, for any pair of class prototypes (μ_{c_1}, μ_{c_2}) , the signed projection of \bar{z}^* onto their connecting direction:

$$\Delta_{c_1, c_2}(\bar{z}^*) = \frac{\langle \bar{z}^* - \frac{\mu_{c_1} + \mu_{c_2}}{2}, \mu_{c_1} - \mu_{c_2} \rangle}{\|\mu_{c_1} - \mu_{c_2}\|_2}.$$

Intuitively, Δ_{c_1, c_2} measures how far (signed) the cluster center sits from the mid-hyperplane between classes c_1 and c_2 .

PROPOSITION 2 (BAND INCLUSION). Assume (i) class prototypes exhibit angular separability $\max_{c \neq c'} \cos(\mu_c, \mu_{c'}) \leq \gamma < 1$, (ii) the aggregation objective satisfies $\mathcal{L}_{\text{agg}}(\varphi^*) \leq \varepsilon$, yielding a radius bound $r \leq R(\varepsilon)$,³ and (iii) (prototype balance) $\max_{c_1, c_2} |\Delta_{c_1, c_2}(\bar{z}^*)| \leq \kappa$. Then for every triggered feature $z'_i \in \mathcal{Z}^*$ and for every pair (c_1, c_2) ,

$$\left| \langle z'_i - \frac{\mu_{c_1} + \mu_{c_2}}{2}, \frac{\mu_{c_1} - \mu_{c_2}}{\|\mu_{c_1} - \mu_{c_2}\|_2} \rangle \right| \leq \kappa + R(\varepsilon),$$

i.e. $z'_i \in \mathcal{B}_{\tilde{\varepsilon}}(c_1, c_2)$ with $\tilde{\varepsilon} = \kappa + R(\varepsilon)$ simultaneously for all class pairs. We refer to $\mathcal{B}_{\tilde{\varepsilon}} = \bigcap_{c_1 < c_2} \mathcal{B}_{\tilde{\varepsilon}}(c_1, c_2)$ as the **multi-class ambiguous band** induced by the trigger.

Discussion. Proposition 2 formalizes that **bounded aggregation** (small $R(\varepsilon)$) plus **prototype balance** (small κ) suffices to place all triggered features inside a uniformly thin, inter-class low-density band. Unlike classical prototype alignment (which explicitly drives z'_i toward a single $\mu_{y'}$), our optimization neither collapses onto any prototype nor requires explicit repulsion terms, and the mixed-class mini-batch implicitly penalizes prototype bias, keeping κ small.

4.3 Attack Workflow

Figure 3 sketches our two-stage pipeline. Below we keep only the high-level intuition, all rigorous derivations, hyper-parameter bounds, and convergence proofs are deferred to Appendix C.

³Because \mathcal{L}_{agg} is the empirical mean of pairwise ℓ_2 distances, a standard concentration (or a worst-case Markov bound combined with mini-batch repetition) gives $R(\varepsilon) = O(\varepsilon)$ in practice; we empirically log r to verify $R(\varepsilon) \ll \text{diam}(\cup_c \mathcal{Z}_c)$.

Stage 1: Trigger Optimization. Starting from a random pattern φ , we minimize the class-agnostic aggregation loss Equation 8 under the perceptual constraint $\|\varphi\|_{\infty} \leq \delta$: $\varphi^* = \text{argmin}_{\|\varphi\|_{\infty} \leq \delta} \mathcal{L}_{\text{agg}}(\varphi)$ (see Algorithm 1 and Appendix C). The resulting feature cloud $\mathcal{Z}^* := \{F_{\theta}(t(x; \varphi^*))\}$ lies inside a thin multi-class band $\mathcal{B}_{\tilde{\varepsilon}}$, regardless of the true label (Proposition 2); thus the **same trigger** transfers to unseen tasks and black-box victims.

Stage 2: Attack Execution. The adversary now deploys only $k \ll N$ triggered samples into the victim’s training set. Two practical variants are supported:

- **Dirty-label Attack.** The adversary flips each selected boundary sample to the target label y' before attaching φ^* . The aligned gradients pull the decision hyper-plane toward $\mathcal{B}_{\tilde{\varepsilon}}$, achieving effective attack success with an $O(k/N)$ clean-accuracy drop.
- **Clean-label Attack.** The adversary keeps the original labels but attach φ^* . Class regions bulge outward to cover the band, yielding the same exponential ASR guarantee while preserving label consistency in the poisoned set.

In both cases the combined effect realises the boundary-relabel principle formalised in Proposition 1–2, and the trigger remains visually imperceptible by design.

5 Evaluation

5.1 Experimental Setup

General Settings. We conduct a comprehensive evaluation of our proposed method, *Eminence*, on a range of widely used vision benchmarks and model architectures. The primary architectures tested include CNNs, like ResNet-18 [19], ResNet-34 [19], and VGG13-BN [49], and transformer-based models such as ViT [8], SimpleViT [2], and CCT [18]. Experiments are performed across CIFAR-10 [24], CIFAR-100 [24], and TinyImageNet [25] datasets. Details of all baseline attacks are summarized in Table 1.

Attack Settings & Evaluation Metrics. Unless otherwise stated, ResNet-18 and CIFAR-10 serve as the default target model and dataset, with all experiments conducted at a 0.01% poison rate. In the white-box scenario, the attacker optimizes the trigger using the same architecture and data as the victim; in the black-box case, model architectures are deliberately misaligned between attacker and victim. Performance is measured via three metrics:

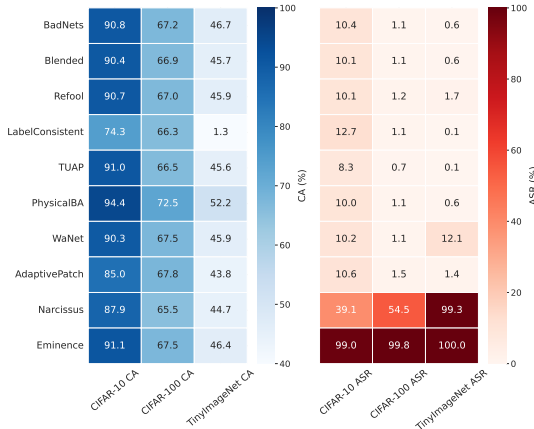
- **Clean Accuracy (CA).** Classification accuracy of the backdoored model on benign (unpoisoned) samples. Higher CA indicates lower impact on the model’s original task.
- **Accuracy Drop (ACC Drop).** $\text{ACC Drop} = \text{CA}_{\text{backdoor}} - \text{CA}_{\text{clean}}$. Higher ACC Drop indicates less degradation to the original task.
- **Attack Success Rate (ASR).** Proportion of triggered samples that are misclassified into the chosen target class. Higher ASR reflects stronger backdoor effectiveness.

5.2 Attack Performance

Effectiveness on CNN Architectures. Table 2 shows that *Eminence* achieves consistently high ASR ($> 99\%$) across all CNN backbones and datasets under both clean- and dirty-label strategies, while clean accuracy remains virtually unchanged with ACC

Table 2: Attack performance of *Eminence* on standard CNN models under various threat scenarios and label settings. Each cell reports ACC Drop (left, (↓))/ASR (right, (↑)).

Dataset	Scenario	ResNet18		ResNet34		VGG13-BN	
		Dirty-label	Clean-label	Dirty-label	Clean-label	Dirty-label	Clean-label
CIFAR10	White-box	-0.1%/99.4%	+0.3%/99.8%	-0.3%/99.9%	-0.1%/94.7%	+0.1%/99.4%	+0.1%/94.3%
	Gray-box	-0.1%/99.9%	+0.2%/96.2%	-0.1%/100.0%	-0.1%/99.9%	+0.1%/100.0%	+0.0%/100.0%
	Black-box	-1.0%/99.9%	-0.9%/99.0%	-1.9%/99.9%	-1.2%/99.9%	-0.9%/99.9%	-0.6%/100.0%
CIFAR100	White-box	-0.3%/99.3%	-0.1%/99.9%	-0.1%/99.6%	-1.0%/99.9%	+0.3%/99.8%	+0.2%/100.0%
	Gray-box	+0.2%/99.9%	+0.9%/99.8%	-0.2%/100.0%	-1.3%/99.8%	+0.5%/99.7%	+0.3%/99.4%
	Black-box	-1.5%/99.9%	-1.5%/99.8%	-3.0%/99.9%	-3.6%/99.9%	-2.6%/100.0%	-2.4%/100.0%
TinyImageNet	White-box	-5.2%/99.7%	-5.5%/99.9%	-7.6%/99.7%	-5.7%/98.9%	-3.4%/99.7%	-3.4%/99.9%
	Gray-box	-4.6%/99.8%	-4.9%/99.9%	-4.4%/100.0%	-4.8%/99.8%	-2.6%/99.8%	-3.2%/100.0%
	Black-box	-4.8%/100.0%	-4.4%/100.0%	-5.1%/100.0%	-4.9%/100.0%	-2.2%/100.0%	-2.7%/100.0%

**Figure 4: Visual comparison of original (benign) and poisoned samples under *Eminence*.****Figure 5: Comparison of CA and ASR for *Eminence* and existing SOTA backdoor attacks across datasets.**

Drop often near zero. In white- and gray-box scenarios, ASR nearly reaches 100% for CIFAR-10/100 with negligible utility loss, and even in challenging black-box settings, *Eminence* sustains 94.0–100.0% ASR, highlighting its resilience to model and data mismatches and stable performance across diverse threat scenarios, suggesting its effectiveness could extend to more realistic deployment environments.

Effectiveness on Transformer Architectures. Table 3 shows that *Eminence* achieves >99% ASR on leading transformer-based architectures in white-box settings with negligible or even slightly positive impact on clean accuracy. In gray- and black-box scenarios, ASR remains high (typically >90%, often >97%) with ACC Drop mostly within $\pm 1\%$, evidencing that **our attack does not rely on**

model-specific artifacts, but rather exploits universal weaknesses at the decision boundary. Such strong transferability not only confirms the theoretical design but also highlights the practical threat posed to contemporary vision models, including those considered more robust due to their architectural novelty.

Attack Visualization. Figure 4 displays benign and poisoned samples under *Eminence*. The poisoned inputs are visually indistinguishable from the clean samples, demonstrating the high stealthiness of our trigger. This qualitative result confirms that *Eminence* can embed a highly effective backdoor while preserving perceptual similarity, further underscoring its practical risk in real-world systems.

5.3 Attack Comparison

As shown in Table 1 and Figure 5, *Eminence* achieves outstanding performance across datasets, reaching a CA of 91.1% and an ASR of 99.0%, which surpasses the next best method Narcissus (ASR 39.1%) by a large margin. The advantage is even more pronounced on CIFAR-100 and TinyImageNet, where *Eminence* consistently sustains both high CA and ASR (>99.8% ASR with minimal utility drop), while most competing attacks fail to exceed 1% ASR. Moreover, unlike classic backdoor attacks such as BadNets, Blended, and WaNet that require poison rates of 0.5%–7%, *Eminence* achieves these results with a poison rate as low as 0.01%, an order of magnitude lower than the strongest prior methods. This confirms that our method not only maintains model utility but also achieves superior attack efficiency, sharply distinguishing it from existing techniques.

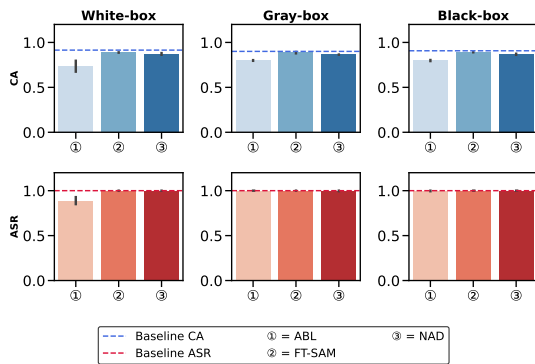
5.4 Defense Study

We evaluate the stealth and robustness of *Eminence* under advanced model-based and input-based backdoor defenses, as described in Section 2.3, providing a realistic measure of its practical risk.

Model-based Mitigation Robustness. Figure 6 summarizes the effects of leading mitigation techniques (ABL [28], FT-SAM [59], NAD [29]) on the attack. *Eminence* remains highly robust against all three defenses, with ASR generally retained high. Even when mitigation reduces CA, the ASR remains above 85%. For FT-SAM and NAD, both CA and ASR remain high, indicating that neither fine-tuning methods like FT-SAM nor adversarial unlearning approaches like ABL are sufficient to neutralize the attack. Such robustness arises from the fact that our approach manipulates the model’s

Table 3: Attack performance of *Eminence* on transformer-based models under various threat scenarios and label settings. In gray- and black-box settings, a ResNet-34 surrogate is used for trigger optimization.

Dataset	Scenario	ViT		SimpleViT		CCT	
		Dirty-label	Clean-label	Dirty-label	Clean-label	Dirty-label	Clean-label
CIFAR10	White-box	-0.7%/99.9%	+0.4%/97.3%	-0.5%/99.4%	+0.0%/93.8%	-0.2%/98.5%	+0.0%/96.2%
	Gray-box	+0.0%/93.5%	-0.5%/91.2%	-0.2%/97.4%	+0.2%/90.3%	+0.0%/95.4%	+0.0%/90.2%
	Black-box	-1.1%/92.7%	+0.1%/90.2%	-0.3%/96.6%	+0.2%/90.2%	-0.1%/92.4%	-0.2%/88.1%
CIFAR100	White-box	+0.5%/100.0%	+0.5%/99.9%	+0.7%/99.9%	+0.4%/99.4%	+0.7%/100.0%	+0.9%/99.9%
	Gray-box	+0.4%/92.1%	+0.1%/90.3%	+0.5%/96.7%	+0.5%/96.0%	+1.2%/91.6%	+0.8%/94.6%
	Black-box	+0.6%/91.3%	+0.6%/87.4%	-0.3%/96.2%	-0.4%/96.3%	+0.0%/91.9%	-0.4%/93.2%
TinyImageNet	White-box	-0.4%/100.0%	-1.0%/100.0%	-1.5%/100.0%	-0.9%/99.9%	-1.3%/100.0%	-1.0%/100.0%
	Gray-box	-0.5%/98.6%	-0.1%/93.8%	-1.2%/97.4%	-1.0%/96.0%	-1.0%/99.8%	-0.3%/98.2%
	Black-box	-0.9%/97.1%	-0.2%/90.7%	-0.6%/97.2%	-0.7%/91.0%	-0.3%/99.6%	-0.3%/97.9%

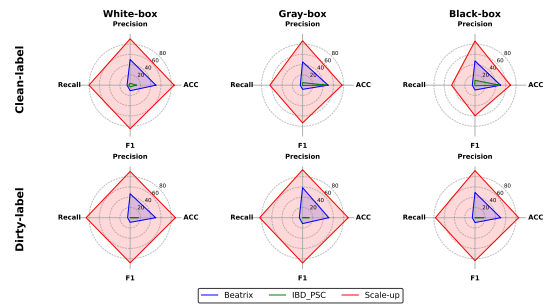
**Figure 6: Impact of model-based mitigation defenses on CA and ASR of *Eminence* across scenarios.**

feature embedding topology, rather than simply introducing easily removable artifacts.

Input-based Detection Stealthiness. Detection results are reported in Figure 7 for Beatrix [35], IBD-PSC [21], and Scale-up [16]. *Eminence* largely evades detection by Beatrix and IBD-PSC, with extremely low recall (typically <10%) and F1 (often near zero). Scale-up, which is specifically tuned to aggressive settings, achieves higher recall and F1. However, this is largely an artifact of Scale-up’s aggressive design and assumptions, and its practical utility diminishes in realistic settings with much lower poison rates, where the detection power drops significantly. These results collectively illustrate the high stealthiness of *Eminence*: while its triggers are highly effective, they are extremely difficult to detect using current mainstream input-based defenses.

5.5 Ablation Study

To further analyze the critical factors influencing the effectiveness and stealthiness of *Eminence*, we perform extensive ablation studies on two key parameters: the noise attaching weight and the number of surrogate samples attacker utilized during trigger optimization. **Impact of Noise Weight.** The noise weight α in Equation 9 regulates the trigger’s intensity, directly mediating the trade-off between attack success and visual stealth. Figure 8a reports the relationship between the noise weight applied to the trigger and the resultant

**Figure 7: Detection performance of *Eminence* against input-based defenses across scenarios. Metrics include accuracy (ACC), precision, recall, and F1 score.**

model performance. We systematically vary the noise weight from 0.05 to 0.2, and record the corresponding ACC Drop and ASR. Empirical results reveal a clear trend: as the noise weight increases, ASR improves rapidly and saturates close to 100%. For instance, at a minimal noise weight of 0.05, the mean ASR remains relatively modest, indicating that the trigger is difficult for the model to memorize in this extreme stealth regime. As the weight is increased to 0.1, 0.15, and especially 0.2, the ASR rises sharply, while the ACC Drop remains low. This demonstrates that *Eminence* can achieve a highly effective backdoor effect even when the trigger is attached almost imperceptibly, balancing stealth and efficacy.

Impact of Surrogate Sample Scale. The surrogate sample scale quantifies the adversary’s data resources, measured as the fraction of the surrogate dataset \mathcal{D}_{atk} compared to the total training dataset $\mathcal{D}_{\text{train}}$, as introduced in Section 3.2. To capture both low-resource and moderately informed adversaries, We also assess the influence of the surrogate samples number attacker used during trigger optimization, as Figure 8b shows. Experimental settings range from using as little as 5% of the available data up to 20%. Results show that even at the lowest sample ratios, the attack remains highly effective, with ASR typically above 90% and only minor drops in CA. As the surrogate sample fraction increases, ASR quickly approaches its theoretical maximum, with little impact on the benign accuracy. For example, with just 5% of samples, *Eminence* achieves ASR values in the 89.9–92.5% range with low ACC drop. At 15–20% samples,

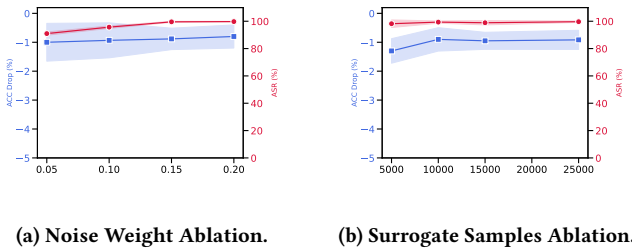


Figure 8: Ablation study of *Eminence*. (a) Impact of trigger noise weight. (b) Impact of the number of surrogate samples used for trigger optimization. The blue line indicates ACC Drop, and the red line denotes ASR.

the ASR reliably reaches 99.5–100.0%, and clean accuracy is effectively preserved. These findings confirm the data efficiency and practicality of our method: it can mount strong attacks even when the attacker’s knowledge or data access is severely constrained.

These ablations show that *Eminence* delivers highly effective and stealthy backdoor attacks even under constrained conditions, consistently outperforming prior SOTA methods.

6 Conclusion

We have introduced a principled, boundary-seeking backdoor framework that unifies theoretical analysis with practical attack design. By characterizing a closed-form “*ambiguous boundary region*”, and quantifying its leverage through influence functions, we showed both analytically and empirically that relabelling only a handful of margin samples is sufficient to steer the decision surface while preserving benign accuracy. Leveraging this insight, our *Eminence* pipeline learns a single, visually subtle trigger that generalizes across clean- and dirty-label settings, transfers to unseen architectures, and attains high attack success with low poison budgets, an order of magnitude smaller than prior SOTA methods, while incurring negligible utility loss. Extensive evaluations confirm the robustness and stealth of the *Eminence*.

Acknowledgment

This work was partly supported by NSFC under No. U244120033, U24A20336, 62172243, 62402425 and 62402418, the China Postdoctoral Science Foundation under No. 2024M762829, the Zhejiang Provincial Natural Science Foundation under No. LD24F020002, the “Pioneer and Leading Goose” R&D Program of Zhejiang under No. 2025C02033 and 2025C01082, and the Zhejiang Provincial Priority-Funded Postdoctoral Research Project under No. ZJ2024001.

References

- [1] Stephen Balaban. 2015. Deep Learning and Face Recognition: The State of the Art. In *Biometric and Surveillance Technology for Human and Activity Identification XII*. Ioannis A. Kakadiaris, Ajay Kumar, and Walter J. Scheirer (Eds.), Vol. 9457. International Society for Optics and Photonics, SPIE, 94570B. doi:10.1117/12.2181526
- [2] Lucas Beyer, Xiaohua Zhai, and Alexander Kolesnikov. 2022. Better Plain ViT Baselines for ImageNet-1k. arXiv:2205.01580 [cs.CV] <https://arxiv.org/abs/2205.01580>
- [3] Bochuan Cao, Jinyuan Jia, Chuxuan Hu, Wenbo Guo, Zhen Xiang, Jinghui Chen, Bo Li, and Dawn Song. 2024. Data Free Backdoor Attacks. In *Advances in Neural Information Processing Systems (NeurIPS)*.
- [4] Jiahao Chen, Zhiqiang Shen, Yuwen Pu, Chunyi Zhou, Changjiang Li, Jiliang Li, Ting Wang, and Shouling Ji. 2024. Rethinking the Vulnerabilities of Face Recognition Systems: From a Practical Perspective. *arXiv preprint arXiv:2405.12786* (2024).
- [5] Xinyun Chen, Chang Liu, Bo Li, Kimberly Lu, and Dawn Song. 2017. Targeted Backdoor Attacks on Deep Learning Systems Using Data Poisoning. *arXiv preprint arXiv:1712.05526* (2017).
- [6] Edward Chou, Florian Tramèr, Giancarlo Pellegrino, and Dan Boneh. 2018. SentiNet: Detecting Physical Attacks Against Deep Learning Systems. *arXiv preprint arXiv:1812.00292* (2018).
- [7] Mark Diaz, Ian Kivlichan, Rachel Rosen, Dylan Baker, Razvan Amironesei, Vinodkumar Prabhakaran, and Remi Denton. 2022. CrowdWorkSheets: Accounting for Individual and Collective Identities Underlying Crowdsourced Dataset Annotation. In *Proceedings of the 2022 ACM Conference on Fairness, Accountability, and Transparency (FACCT) (FACCT ’22)*. Association for Computing Machinery, New York, NY, USA, 2342–2351. doi:10.1145/3531146.3534647
- [8] Alexey Dosovitskiy, Lucas Beyer, Alexander Kolesnikov, Dirk Weissenborn, Xi-aohua Zhai, Thomas Unterthiner, Mostafa Dehghani, Matthias Minderer, Georg Heigold, Sylvain Gelly, Jakob Uszkoreit, and Neil Houlsby. 2021. An Image Is Worth 16x16 Words: Transformers for Image Recognition at Scale. In *Proceedings of the 9th International Conference on Learning Representations (ICLR)*. OpenReview.net. <https://openreview.net/forum?id=YicbFdNTTy>
- [9] Jacob Dumford and Walter J. Scheirer. 2020. Backdooring Convolutional Neural Networks via Targeted Weight Perturbations. In *Proc. IEEE Int. Joint Conf. Biometrics (IJCB)*. 1–9.
- [10] Zhou Feng, Jiahao Chen, Chunyi Zhou, Yuwen Pu, Qingming Li, and Shouling Ji. 2025. Poison in the Well: Feature Embedding Disruption in Backdoor Attacks. In *Proc. IEEE Int. Conf. Multimedia and Expo (ICME)*. doi:10.1109/ICME59968.2025.11209199
- [11] Pierre Foret, Ariel Kleiner, Hossein Mobahi, and Behnam Neyshabur. 2021. Sharpness-Aware Minimization for Efficiently Improving Generalization. In *Proc. Int. Conf. Learn. Represent. (ICLR)*.
- [12] Yansong Gao, Yeonjae Kim, Bao Gia Doan, Zhi Zhang, Gongxuan Zhang, Surya Nepal, Damith C. Ranasinghe, and Hyoungshick Kim. 2022. Design and Evaluation of a Multi-Domain Trojan Detection Method on Deep Neural Networks. *IEEE Trans. Dependable Secure Comput.* 19, 4 (2022), 2349–2364.
- [13] Yansong Gao, Change Xu, Derui Wang, Shiping Chen, Damith C. Ranasinghe, and Surya Nepal. 2019. STRIP: A Defence Against Trojan Attacks on Deep Neural Networks. In *Proc. Annu. Comput. Secur. Appl. Conf. (ACSAC)*. 113–125.
- [14] Siddhant Garg, Adarsh Kumar, Vibhor Goel, and Yingyu Liang. 2020. Can Adversarial Weight Perturbations Inject Neural Backdoors. In *Proc. ACM Int. Conf. Inf. Knowl. Manag. (CIKM)*. 2029–2032.
- [15] Tianyu Gu, Brendan Dolan-Gavitt, and Siddharth Garg. 2017. BadNets: Identifying Vulnerabilities in the Machine Learning Model Supply Chain. *arXiv preprint arXiv:1708.06733* (2017).
- [16] Junfeng Guo, Yiming Li, Xun Chen, Hanqing Guo, Lichao Sun, and Cong Liu. 2023. SCALE-UP: An Efficient Black-box Input-level Backdoor Detection via Analyzing Scaled Prediction Consistency. In *Proc. Int. Conf. Learn. Represent. (ICLR)*.
- [17] Lucjan Hanzlik, Yang Zhang, Kathrin Grosse, Ahmed Salem, Maximilian Augustin, Michael Backes, and Mario Fritz. 2021. MLCapsule: Guarded Offline Deployment of Machine Learning as a Service. In *Proceedings of the IEEE/CVF Conference on Computer Vision and Pattern Recognition (CVPR) Workshops*. IEEE, 3300–3309.
- [18] Ali Hassani, Steven Walton, Nikhil Shah, Abulikemu Abuduweili, Jiachen Li, and Humphrey Shi. 2021. Escaping the Big Data Paradigm with Compact Transformers. arXiv:2104.05704 [cs.CV] <https://arxiv.org/abs/2104.05704>
- [19] Kaiming He, Xiangyu Zhang, Shaoqing Ren, and Jian Sun. 2016. Deep Residual Learning for Image Recognition. In *Proceedings of the IEEE Conference on Computer Vision and Pattern Recognition (CVPR)*. IEEE, 770–778.
- [20] Junyuan Hong, Lingjuan Lyu, Jiayu Zhou, and Michael Spranger. 2022. Outsourcing Training without Uploading Data via Efficient Collaborative Open-Source Sampling. In *Proceedings of the 36th Conference on Neural Information Processing Systems (NeurIPS)*, Vol. 35. Curran Associates, Inc., 20133–20146. https://proceedings.neurips.cc/paper_files/paper/2022/file/7efe88bb4138d602e56637cfcf713654-Paper-Conference.pdf
- [21] Linshan Hou, Ruili Feng, Zhongyun Hua, Wei Luo, Leo Yu Zhang, and Yiming Li. 2024. IB-D-PSC: Input-level Backdoor Detection via Parameter-oriented Scaling Consistency. In *Proc. Int. Conf. Mach. Learn. (ICML)*. 764.
- [22] Zhitao Huang, Peipeng Yu, Zhihua Xia, Xi Yang, and Run Lu. 2025. IdentityLock: An Identity-Aware Backdoor Strategy for Face Swapping Defense. In *Proceedings of the IEEE International Conference on Acoustics, Speech and Signal Processing (ICASSP)*. IEEE, 1–5. doi:10.1109/ICASSP49660.2025.10890392
- [23] Moaiad Ahmad Khder. 2021. Web Scraping or Web Crawling: State of Art, Techniques, Approaches and Application. *International Journal of Advances in Soft Computing & Its Applications* 13, 3 (2021).
- [24] Alex Krizhevsky and Geoffrey Hinton. 2009. *Learning Multiple Layers of Features from Tiny Images*. Technical Report. University of Toronto, Toronto, ON, Canada. Technical Report.

- [25] Ya Le and Xuan Yang. 2015. Tiny ImageNet Visual Recognition Challenge. <https://tinyimagenet.com>. CS231n Course Project, Stanford University.
- [26] Yuanchun Li, Jiayi Hua, Haoyu Wang, Chunyang Chen, and Yunxin Liu. 2021. DeepPayload: Black-box Backdoor Attack on Deep Learning Models through Neural Payload Injection. In *Proc. Int. Conf. Softw. Eng. (ICSE)*. 263–274.
- [27] Yiming Li, Yong Jiang, Zhifeng Li, and Shu-Tao Xia. 2024. Backdoor Learning: A Survey. *IEEE Transactions on Neural Networks and Learning Systems* 35, 1 (2024), 5–22. doi:10.1109/TNNLS.2022.3182979
- [28] Yige Li, Xixiang Lyu, Nodens Koren, Lingjuan Lyu, Bo Li, and Xingjun Ma. 2021. Anti-Backdoor Learning: Training Clean Models on Poisoned Data. In *Advances in Neural Information Processing Systems (NeurIPS)*. 14900–14912.
- [29] Yige Li, Xixiang Lyu, Nodens Koren, Lingjuan Lyu, Bo Li, and Xingjun Ma. 2021. Neural Attention Distillation: Erasing Backdoor Triggers from Deep Neural Networks. In *Proc. Int. Conf. Learn. Represent. (ICLR)*.
- [30] Yiming Li, Tongqing Zhai, Yong Jiang, Zhifeng Li, and Shu-Tao Xia. 2021. Backdoor Attack in the Physical World. *arXiv preprint arXiv:2104.02361* (2021).
- [31] Timothy Libert. 2018. An Automated Approach to Auditing Disclosure of Third-Party Data Collection in Website Privacy Policies. In *Proceedings of the 2018 World Wide Web Conference (WWW) (WWW '18)*. International World Wide Web Conferences Steering Committee, Republic and Canton of Geneva, Switzerland, 207–216. doi:10.1145/3178876.3186087
- [32] Xiaogeng Liu, Minghui Li, Haoyu Wang, Shengshan Hu, Dengpan Ye, Hai Jin, Libing Wu, and Chaowei Xiao. 2023. Detecting Backdoors During the Inference Stage Based on Corruption Robustness Consistency. In *Proc. IEEE Conf. Comput. Vis. Pattern Recognit. (CVPR)*. 16363–16372.
- [33] Yunfei Liu, Xingjun Ma, James Bailey, and Feng Lu. 2020. Reflection Backdoor: A Natural Backdoor Attack on Deep Neural Networks. In *Proc. Eur. Conf. Comput. Vis. (ECCV)*. 182–199.
- [34] Peizhuo Lv, Chang Yue, Ruigang Liang, Yunfei Yang, Shengzhi Zhang, Hualong Ma, and Kai Chen. 2023. A Data-free Backdoor Injection Approach in Neural Networks. In *Proc. USENIX Security Symp.* 2671–2688.
- [35] Wanlun Ma, Derui Wang, Ruoxi Sun, Minhui Xue, Sheng Wen, and Yang Xiang. 2023. The "Beatrix" Resurrections: Robust Backdoor Detection via Gram Matrices. In *Proc. Netw. Distrib. Syst. Secur. Symp. (NDSS)*.
- [36] Preeti Nagrath, Rachna Jain, Agam Madan, Rohan Arora, Piyush Kataria, and Jude Hemanth. 2021. SSDMNV2: A Real Time DNN-Based Face Mask Detection System Using Single Shot Multibox Detector and MobileNetV2. *Sustainable Cities and Society* 66 (2021), 102692. doi:10.1016/j.scs.2020.102692
- [37] Tuan Anh Nguyen and Anh Tuan Tran. 2021. WaNet – Imperceptible Warping-based Backdoor Attack. In *Proc. Int. Conf. Learn. Represent. (ICLR)*.
- [38] Soumyadeep Pal, Yuguang Yao, Ren Wang, Bingquan Shen, and Sijia Liu. 2024. Backdoor Secrets Unveiled: Identifying Backdoor Data with Optimized Scaled Prediction Consistency. In *Proc. Int. Conf. Learn. Represent. (ICLR)*.
- [39] Joel B. Predd, Sanjeev R. Kulkarni, and H. Vincent Poor. 2009. A Collaborative Training Algorithm for Distributed Learning. *IEEE Transactions on Information Theory* 55, 4 (2009), 1856–1871. doi:10.1109/TIT.2009.2012992
- [40] Yuwen Pu, Jiahao Chen, Chunyi Zhou, Zhou Feng, Qingming Li, Chunqiang Hu, and Shouling Ji. 2024. Mellivora Capensis: A Backdoor-Free Training Framework on the Poisoned Dataset without Auxiliary Data. *arXiv preprint arXiv:2405.12719* (2024).
- [41] Xiangyu Qi, Tinghao Xie, Yiming Li, Saeed Mahloujifar, and Prateek Mittal. 2023. Revisiting the Assumption of Latent Separability for Backdoor Defenses. In *Proc. Int. Conf. Learn. Represent. (ICLR)*.
- [42] Xiangyu Qi, Tinghao Xie, Ruizhe Pan, Jifeng Zhu, Yong Yang, and Kai Bu. 2022. Towards Practical Deployment-Stage Backdoor Attack on Deep Neural Networks. In *Proc. IEEE Conf. Comput. Vis. Pattern Recognit. (CVPR)*. 13337–13347.
- [43] Xiangyu Qi, Tinghao Xie, Jiachen T. Wang, Tong Wu, Saeed Mahloujifar, and Prateek Mittal. 2023. Towards a Proactive ML Approach for Detecting Backdoor Poison Samples. In *Proc. USENIX Security Symp.* 1685–1702.
- [44] Adnan Siraj Rakin, Zhezhi He, and Deliang Fan. 2020. TBT: Targeted Neural Network Attack With Bit Trojan. In *Proc. IEEE Conf. Comput. Vis. Pattern Recognit. (CVPR)*. 13195–13204.
- [45] Ratheesh Ravindran, Michael J. Santora, and Mohsin M. Jamali. 2021. Multi-Object Detection and Tracking, Based on DNN, for Autonomous Vehicles: A Review. *IEEE Sensors Journal* 21, 5 (2021), 5668–5677. doi:10.1109/JSEN.2020.3041615
- [46] Mauro Ribeiro, Katarina Grolinger, and Miriam A. M. Capretz. 2015. MLaaS: Machine Learning as a Service. In *Proceedings of the 2015 IEEE 14th International Conference on Machine Learning and Applications (ICMLA)*. IEEE, 896–902. doi:10.1109/ICMLA.2015.152
- [47] Yuji Roh, Geon Heo, and Steven Euijong Whang. 2021. A Survey on Data Collection for Machine Learning: A Big Data - AI Integration Perspective. *IEEE Transactions on Knowledge and Data Engineering* 33, 4 (2021), 1328–1347. doi:10.1109/TKDE.2019.2946162
- [48] Aniruddha Saha, Akshayvarun Subramanya, and Hamed Pirsiavash. 2020. Hidden Trigger Backdoor Attacks. In *Proc. AAAI Conf. Artif. Intell. (AAAI)*. 11957–11965.
- [49] Karen Simonyan and Andrew Zisserman. 2015. Very Deep Convolutional Networks for Large-Scale Image Recognition. *arXiv:1409.1556 [cs.CV]* <https://arxiv.org/abs/1409.1556> arXiv:1409.1556.
- [50] Hossein Souri, Liam Fowl, Rama Chellappa, Micah Goldblum, and Tom Goldstein. 2022. Sleeper Agent: Scalable Hidden Trigger Backdoors for Neural Networks Trained from Scratch. In *Advances in Neural Information Processing Systems (NeurIPS)*.
- [51] Ruixiang Tang, Mengnan Du, Ninghao Liu, Fan Yang, and Xia Hu. 2020. An Embarrassingly Simple Approach for Trojan Attack in Deep Neural Networks. In *Proc. ACM SIGKDD Conf. Knowl. Discov. Data Min. (KDD)*. 218–228.
- [52] Alexander Turner, Dimitris Tsipras, and Aleksander Madry. 2019. Label-Consistent Backdoor Attacks. *arXiv preprint arXiv:1912.02771* (2019).
- [53] Bolun Wang, Yuanshun Yao, Shawn Shan, Huiying Li, Bimal Viswanath, Haitao Zheng, and Ben Y. Zhao. 2019. Neural Cleanse: Identifying and Mitigating Backdoor Attacks in Neural Networks. In *Proc. IEEE Symp. Secur. Privacy (S&P)*. 707–723.
- [54] Karl Weiss, Taghi M. Khoshgoftaar, and DingDing Wang. 2016. A Survey of Transfer Learning. *Journal of Big Data* 3, 1 (2016), 9. doi:10.1186/s40537-016-0043-6
- [55] Ekim Yurtsever, Jacob Lambert, Alexander Carballo, and Kazuya Takeda. 2020. A Survey of Autonomous Driving: Common Practices and Emerging Technologies. *IEEE Access* 8 (2020), 58443–58469. doi:10.1109/ACCESS.2020.2983149
- [56] Yi Zeng, Si Chen, Won Park, Zhuoqing Mao, Ming Jin, and Ruoxi Jia. 2022. Adversarial Unlearning of Backdoors via Implicit Hypergradient. In *Proc. Int. Conf. Learn. Represent. (ICLR)*.
- [57] Yi Zeng, Minzhou Pan, Hoang Anh Just, Lingjuan Lyu, Meikang Qiu, and Ruoxi Jia. 2023. Narcissus: A Practical Clean-Label Backdoor Attack with Limited Information. In *Proc. ACM Conf. Comput. Commun. Secur. (CCS)*. 771–785.
- [58] Shihao Zhao, Xingjun Ma, Xiang Zheng, James Bailey, Jingjing Chen, and Yu-Gang Jiang. 2020. Clean-Label Backdoor Attacks on Video Recognition Models. In *Proc. IEEE Conf. Comput. Vis. Pattern Recognit. (CVPR)*. 14431–14440.
- [59] Mingli Zhu, Shaokui Wei, Li Shen, Yanbo Fan, and Baoyuan Wu. 2023. Enhancing Fine-Tuning Based Backdoor Defense with Sharpness-Aware Minimization. In *Proc. IEEE Int. Conf. Comput. Vis. (ICCV)*. 4443–4454.

A Proof of Proposition 1

Assumptions. We clarify and refine the assumptions under the original notation system as follows:

- (1) **Linear Classifier.** $g_\theta(z) = \arg \max_{c \in \mathcal{C}} \langle w_c, z \rangle + b_c$. For simplicity, we absorb the bias b_c into the weights w_c .
- (2) **Bounded Feature & Gradient.** For any input x , its feature norm is bounded: $\|F_\theta(x)\|_2 \leq R$. In addition, we assume the per-sample loss gradient with respect to parameters is bounded: $\|\nabla_\theta \ell(f_\theta(x), y)\|_2 \leq G$.
- (3) **λ_{\min} -strongly Convex Loss.** The loss is defined as

$$\mathcal{L}(\theta) = \frac{1}{N} \sum_i \ell(f_\theta(x_i), y_i),$$

whose Hessian at the clean optimum θ^* satisfies $H_{\theta^*} := \nabla_\theta^2 \mathcal{L}(\theta^*) \succeq \lambda_{\min} I$. This is a strong assumption to ensure the tractability of theoretical analysis.

- (4) **Margin Density Near Zero.** For clean data,

$$\Pr[|m_y(x) - \max_{c \neq y} m_c(x)| \leq t] \leq vt, \quad \forall t \in (0, 1].$$

- (5) **Independent Per-sample Influence.** We model the total parameter change as $\Delta\theta = \sum_{i=1}^k \Delta\theta_i$, where $\Delta\theta_i$ denotes the independent contribution caused by the i -th poisoned sample, and its norm is bounded: $\|\Delta\theta_i\|_2 \leq \beta'$.

Step 1 – Parameter Drift Bound. At the clean model’s optimal parameter θ^* , the gradient of the loss is zero: $\nabla \mathcal{L}(\theta^*) = 0$. Let

$$g := \sum_{x' \in \mathcal{D}_p} \nabla_\theta \ell(f_{\theta^*}(x'), y'),$$

According to influence function analysis, the total parameter drift $\Delta\theta$ caused by k poisoned samples can be approximated by $\Delta\theta \approx$

$-\frac{\eta}{N} H_{\theta^*}^{-1} g$. Using Assumptions 2 and 3, we can bound its norm:

$$\|\Delta\theta\|_2 \leq \frac{\eta}{N} \|H_{\theta^*}^{-1}\|_2 \|g\|_2 \leq \frac{\eta}{N} \cdot \frac{1}{\lambda_{\min}} \cdot (kG),$$

We thus define the parameter drift bound ρ as

$$\boxed{\|\Delta\theta\|_2 \leq \frac{\eta k G}{N \lambda_{\min}} =: \rho.} \quad (11)$$

Step 2 – Exponential Bound on ASR.

(i) *Initial margin and bounded increment.* For any feature z in the ambiguous region $\mathcal{B}_\varepsilon(c^*, y')$, its initial margin satisfies $m_{y'}(z) - m_{c^*}(z) \geq -\varepsilon$. By Assumption 5, the total parameter shift can be seen as a sum of k independent contributions, $\Delta\theta = \sum_{i=1}^k \Delta\theta_i$. The contribution of the i -th sample to the margin is

$$Y_i := \left\langle \Delta w_{y'}^{(i)} - \Delta w_{c^*}^{(i)}, z \right\rangle.$$

The variables $\{Y_i\}$ are independent and bounded: $|Y_i| \leq 2R\beta' =: B$.

(ii) *Concentration.* The attack is constructed so that $\mathbb{E}[Y_i] = \mu > 0$. By Hoeffding's inequality, the probability that the sum $\sum Y_i$ deviates significantly from its mean is exponentially small:

$$\Pr\left[\sum_{i=1}^k Y_i < \frac{k\mu}{2}\right] \leq \exp\left(-\frac{k\mu^2}{8B^2}\right) =: e^{-ck}, \quad \text{where } c = \frac{\mu^2}{8B^2},$$

Thus, $\sum_{i=1}^k Y_i \geq \frac{k\mu}{2}$ holds with probability at least $1 - e^{-ck}$.

(iii) *Margin sign after poisoning.* The new post-attack margin is

$$m'_{y'}(z) - m'_{c^*}(z) = (m_{y'}(z) - m_{c^*}(z)) + \sum_{i=1}^k Y_i \geq -\varepsilon + \frac{k\mu}{2}.$$

As long as $\frac{k\mu}{2} > \varepsilon$, the right side is positive and the classification result flips to y' . Hence, the attack failure probability ξ decays exponentially in k , i.e., $\xi = O(e^{-k})$.

Step 3 – Linear Bound on CA. For a clean sample (x, y) , via Equation 11, the change in the logit for any class c is bounded by:

$$|m'_c(x) - m_c(x)| = |\langle \Delta w_c, F_\theta(x) \rangle| \leq \|\Delta\theta\|_2 R \leq R\rho,$$

Therefore, the post-attack margin $r'(x) = m'_{y'}(x) - \max_{c \neq y} m'_c(x)$ satisfies $r'(x) \geq r(x) - 2R\rho$. The probability γ that the model misclassifies is bounded by

$$\boxed{\gamma = \Pr_{(x,y)} [r'(x) < 0] \leq \Pr[r(x) < 2R\rho] \leq v(2R\rho)}$$

$$\implies \gamma = O(\rho).$$

Step 4 – Conclusion. Combining the above steps, we establish the two core properties of this attack. Let $\theta' = \theta^* + \Delta\theta$:

$$\Pr_{x \sim \mathcal{B}_\varepsilon} [g_{\theta'} \circ F_{\theta'}(x) = y'] \geq 1 - O(e^{-k}), \quad (12)$$

$$\Pr_{(x,y) \sim \mathcal{D}_{\text{clean}}} [g_{\theta'} \circ F_{\theta'}(x) = y] \geq 1 - O(\rho). \quad (13)$$

This demonstrates that the attack success rate grows exponentially with the number of poisoned samples k , while the clean accuracy drop scales linearly with the poisoning ratio k/N and remains controllable. \square

B Proof of Proposition 2

Assumptions. We restate the three conditions in Proposition 2 in a compact form:

- (1) **Angular Separability.** $\max_{c \neq c'} \cos(\mu_c, \mu_{c'}) \leq \gamma < 1$.
- (2) **Bounded Aggregation Radius.** $\mathcal{L}_{\text{agg}}(\varphi^*) \leq \varepsilon$ implies $r := \max_i \|z'_i - \bar{z}^*\|_2 \leq R(\varepsilon)$ for some monotone $R(\cdot)$.
- (3) **Prototype Balance.** $\max_{c_1, c_2} |\Delta_{c_1, c_2}(\bar{z}^*)| \leq \kappa$.

Here $z'_i = F_\theta(t(x_i; \varphi^*))$, \bar{z}^* is their centroid, and

$$\Delta_{c_1, c_2}(\bar{z}^*) = \frac{\left\langle \bar{z}^* - \frac{\mu_{c_1} + \mu_{c_2}}{2}, \mu_{c_1} - \mu_{c_2} \right\rangle}{\|\mu_{c_1} - \mu_{c_2}\|_2}.$$

Step 1 – From \mathcal{L}_{agg} to a Radius Bound. Recall the symmetric variance identity

$$\frac{2}{B(B-1)} \sum_{i < j} \|z'_i - z'_j\|_2^2 = \frac{2}{B-1} \sum_{i=1}^B \|z'_i - \bar{z}^*\|_2^2,$$

Since \mathcal{L}_{agg} upper-bounds (up to a constant) the left-hand side, we obtain

$$\sum_{i=1}^B \|z'_i - \bar{z}^*\|_2^2 \leq \frac{B-1}{2} \mathcal{L}_{\text{agg}}(\varphi^*) \leq \frac{B-1}{2} \varepsilon.$$

Hence

$$r := \max_i \|z'_i - \bar{z}^*\|_2 \leq \sqrt{\frac{B-1}{2} \varepsilon} =: R(\varepsilon),$$

which justifies the existence of a non-decreasing $R(\varepsilon) = O(\sqrt{\varepsilon})$.⁴

Step 2 – Bounding the Center's Signed Distance. For any class pair (c_1, c_2) , define the unit direction

$$u_{c_1, c_2} := \frac{\mu_{c_1} - \mu_{c_2}}{\|\mu_{c_1} - \mu_{c_2}\|_2}.$$

By definition of Δ_{c_1, c_2} ,

$$\left| \left\langle \bar{z}^* - \frac{\mu_{c_1} + \mu_{c_2}}{2}, u_{c_1, c_2} \right\rangle \right| \leq \kappa.$$

This bounds the centre's (signed) offset from the mid-hyperplane.

Step 3 – Triangle Inequality on Projections. For any $z'_i \in \mathcal{Z}^*$,

$$\begin{aligned} & \left| \left\langle z'_i - \frac{\mu_{c_1} + \mu_{c_2}}{2}, u_{c_1, c_2} \right\rangle \right| \\ &= \left| \left\langle (z'_i - \bar{z}^*) + \left(\bar{z}^* - \frac{\mu_{c_1} + \mu_{c_2}}{2} \right), u_{c_1, c_2} \right\rangle \right| \\ &\leq \underbrace{\left| \left\langle z'_i - \bar{z}^*, u_{c_1, c_2} \right\rangle \right|}_{\leq \|z'_i - \bar{z}^*\|_2 \leq r} + \underbrace{\left| \left\langle \bar{z}^* - \frac{\mu_{c_1} + \mu_{c_2}}{2}, u_{c_1, c_2} \right\rangle \right|}_{\leq \kappa} \\ &\leq r + \kappa \leq R(\varepsilon) + \kappa. \end{aligned}$$

Thus, for every pair (c_1, c_2) ,

$$\left| \left\langle z'_i - \frac{\mu_{c_1} + \mu_{c_2}}{2}, u_{c_1, c_2} \right\rangle \right| \leq R(\varepsilon) + \kappa.$$

Step 4 – Band Inclusion & Intersection. By the definition of $\mathcal{B}_{\tilde{\varepsilon}}(c_1, c_2)$, taking $\tilde{\varepsilon} = R(\varepsilon) + \kappa$ gives

$$z'_i \in \mathcal{B}_{\tilde{\varepsilon}}(c_1, c_2), \quad \forall (c_1, c_2).$$

Therefore,

$$z'_i \in \mathcal{B}_{\tilde{\varepsilon}} := \bigcap_{c_1 < c_2} \mathcal{B}_{\tilde{\varepsilon}}(c_1, c_2), \quad \tilde{\varepsilon} = \kappa + R(\varepsilon),$$

⁴When the anchor form is used in practice, one can still bound r by noting the anchor is also within $R(\varepsilon)$ of the centroid with high probability (via mini-batch reshuffling), so the same order bound holds.

which completes the proof. \square

C Trigger-optimization Dynamics

This appendix formalizes *Stage 1: Trigger Optimization* in Section 4.3.

Notations. We detail the aggregation loss:

$$\mathcal{L}_{\text{agg}}(\varphi) = \frac{2}{B(B-1)} \sum_{i < j} \|z_i(\varphi) - z_j(\varphi)\|_2^2.$$

We perform projected gradient descent (PGD) on φ under the ℓ_∞ -constraint:

$$\varphi^{(k+1)} = \Pi_{\|\cdot\|_\infty \leq \delta} \left[\varphi^{(k)} - \eta_k \nabla_{\varphi} \mathcal{L}_{\text{agg}}(\varphi^{(k)}) \right], \quad \eta_k > 0.$$

Assumptions.

- (1) **Feature Lipschitzness.** F_θ is L -Lipschitz and $\|F_\theta(x)\|_2 \leq R_x$ for all x .
- (2) **Bounded Input Scale.** Inputs are rescaled into a compact set so that $t(\cdot; \varphi)$ is α -Lipschitz in φ .

Smoothness of \mathcal{L}_{agg} .

LEMMA 1 (LIPSCHITZ GRADIENT). *Under the above assumptions, \mathcal{L}_{agg} is $4\alpha^2 L^2$ -smooth in φ , i.e.,*

$$\|\nabla \mathcal{L}_{\text{agg}}(\varphi) - \nabla \mathcal{L}_{\text{agg}}(\varphi')\|_2 \leq 4\alpha^2 L^2 \|\varphi - \varphi'\|_2.$$

PROOF. For any φ, φ' , we have

$$\|z_i(\varphi) - z_i(\varphi')\|_2 \leq L \|t(x_i; \varphi) - t(x_i; \varphi')\|_2 \leq \alpha L \|\varphi - \varphi'\|_2.$$

Expanding \mathcal{L}_{agg} and applying standard variance-smoothness arguments yields the claim. \square

Convergence of PGD.

PROPOSITION 3 (PGD CONVERGENCE). *With constant step size $\eta_k = 1/(4\alpha^2 L^2)$, after K steps*

$$\min_{0 \leq k < K} \|\nabla_{\varphi} \mathcal{L}_{\text{agg}}(\varphi^{(k)})\|_2^2 \leq \frac{8\alpha^2 L^2}{K} [\mathcal{L}_{\text{agg}}(\varphi^{(0)}) - \mathcal{L}_{\text{agg}}^*],$$

where $\mathcal{L}_{\text{agg}}^*$ is the minimum over $\|\varphi\|_\infty \leq \delta$. Hence an ε -stationary point is reached in $K = O(\alpha^2 L^2 \varepsilon^{-2})$ iterations.

Sample Complexity for Radius Estimation. Let $R(\varepsilon)$ denote the radius upper bound implied by an ε -optimal value of \mathcal{L}_{agg} (Proposition 2).

LEMMA 2 (CONCENTRATION OF EMPIRICAL RADIUS). *For any $\xi, \delta \in (0, 1)$,*

$$\Pr \left[|R_B(\varepsilon) - R(\varepsilon)| > \xi \right] \leq 2 \exp \left(-\frac{B\xi^2}{8R_x^2} \right).$$

Thus $B = O(R_x^2 \xi^{-2} \log \delta^{-1})$ samples suffice to estimate $R(\varepsilon)$ within ξ with probability $1 - \delta$.

PROOF. Apply Hoeffding's inequality to the empirical variance proxy underlying \mathcal{L}_{agg} . \square

Consequence for Band Inclusion. By Proposition 3 and Lemma 2, a finite PGD schedule attains an ε -approximate minimizer with a reliable radius estimate, and Proposition 2 yields

$$\mathcal{Z}^* \subset \mathcal{B}_{\tilde{\varepsilon}}, \quad \tilde{\varepsilon} = \kappa + R(\varepsilon).$$

Conclusion. Lemma 1 and Proposition 3 ensure stable convergence of trigger optimization, while Lemma 2 controls estimation error,

together with Proposition 2, these results place \mathcal{Z}^* within the desired ambiguous band after finitely many iterations.

D Proof of Proposition 3

Assumptions. We assume:

- (1) **Surrogate-feature Lipschitzness.** The frozen extractor F_θ is L -Lipschitz: $\|F_\theta(x) - F_\theta(x')\|_2 \leq L \|x - x'\|_2$.
- (2) **Trigger Parametrization.** A triggered input is $t(x; \varphi) = (1 - \alpha)x + \alpha\varphi$ with fixed $\alpha \in (0, 1]$.
- (3) **Feasible Set.** $\mathcal{C} := \{\varphi \in \mathbb{R}^{d_x} \mid \|\varphi\|_\infty \leq \delta\}$ is closed and convex; the projection P_C is w.r.t. ℓ_2 norm.
- (4) **Aggregation Loss.** For a mini-batch $\mathcal{D}_B = \{x_i\}_{i=1}^B$,

$$\mathcal{L}_{\text{agg}}(\varphi) = \frac{2}{B(B-1)} \sum_{i < j} \|F_\theta(t(x_i; \varphi)) - F_\theta(t(x_j; \varphi))\|_2^2.$$

- (5) **PGD Step.** $\varphi^{(k+1)} = P_C [\varphi^{(k)} - \eta \nabla \mathcal{L}_{\text{agg}}(\varphi^{(k)})]$ with $\eta = 1/(4\alpha^2 L^2)$.

Let $g^{(k)} := \nabla \mathcal{L}_{\text{agg}}(\varphi^{(k)})$.

Step 1 – Projection Optimality. For the non-expansive projection in Assumption 3,

$$\langle \varphi^{(k)} - \eta g^{(k)} - \varphi^{(k+1)}, \varphi - \varphi^{(k+1)} \rangle \leq 0, \quad \forall \varphi \in \mathcal{C}. \quad (14)$$

Step 2 – Descent Lemma. Take $\varphi = \varphi^{(k)}$ in Equation 14 to obtain

$$\langle g^{(k)}, \varphi^{(k+1)} - \varphi^{(k)} \rangle \leq -\frac{1}{\eta} \|\varphi^{(k+1)} - \varphi^{(k)}\|_2^2. \quad (15)$$

Step 3 – Smoothness Bound. By Lemma 1,

$$\begin{aligned} \mathcal{L}_{\text{agg}}(\varphi^{(k+1)}) &\leq \mathcal{L}_{\text{agg}}(\varphi^{(k)}) + \langle g^{(k)}, \varphi^{(k+1)} - \varphi^{(k)} \rangle \\ &\quad + \frac{L_f}{2} \|\varphi^{(k+1)} - \varphi^{(k)}\|_2^2. \end{aligned} \quad (16)$$

Substituting Equation 15 and $\eta = 1/L_f$ gives

$$\mathcal{L}_{\text{agg}}(\varphi^{(k)}) - \mathcal{L}_{\text{agg}}(\varphi^{(k+1)}) \geq \frac{\eta}{2} \|g^{(k)}\|_2^2. \quad (17)$$

Step 4 – Telescoping. Summing Equation 17 for $k = 0$ to $K - 1$ and telescoping,

$$\frac{\eta}{2} \sum_{k=0}^{K-1} \|g^{(k)}\|_2^2 \leq \mathcal{L}_{\text{agg}}(\varphi^{(0)}) - \mathcal{L}_{\text{agg}}^*,$$

whence

$$\min_{0 \leq k < K} \|g^{(k)}\|_2^2 \leq \frac{2}{\eta K} [\mathcal{L}_{\text{agg}}(\varphi^{(0)}) - \mathcal{L}_{\text{agg}}^*].$$

Step 5 – Iteration Complexity. With $\eta = 1/L_f = 1/(4\alpha^2 L^2)$ the bound becomes

$$\min_{k < K} \|\nabla \mathcal{L}_{\text{agg}}(\varphi^{(k)})\|_2^2 \leq \frac{8\alpha^2 L^2}{K} [\mathcal{L}_{\text{agg}}(\varphi^{(0)}) - \mathcal{L}_{\text{agg}}^*].$$

Requiring the RHS $\leq \varepsilon^2$ yields $K \geq 8\alpha^2 L^2 [\mathcal{L}_{\text{agg}}(\varphi^{(0)}) - \mathcal{L}_{\text{agg}}^*] / \varepsilon^2 = O(\alpha^2 L^2 \varepsilon^{-2})$, completing the proof. \square